Simulating particle acceleration in rippled space plasma shocks

Master's Thesis
University of Turku
Dept. of Physics and Astronomy
Physics
2020
Frans Sjöblom
Supervised by:
Docent Heli Hietala
Dr. Alexandr Afanaisev
Reviewed by:
Professor Rami Vainio
Dr. Alexandr Afanasiev

The originality of this thesis has been checked in accordance with the University of Turku quality assurance system using the Turnitin OriginalityCheck service

UNIVERSITY OF TURKU
Department of Physics and Astronomy
SJÖBLOM, FRANS Simulating particle acceleration in rippled space plasma shocks

Master's Thesis, 42 p.
Physics
May 2020
The originality of this thesis has been checked in accordance with the University of Turku quality assurance system using the Turnitin OriginalityCheck service

---

Plasma shocks are one of the key mechanisms accelerating particles to high energies. Although the theory behind diffusive shock acceleration is well known, there are unexplained differences in the observed particle spectra of different shock geometries. Recently with multispacecraft missions like Cluster, Time History of Events and Macroscale Interactions during Substorms (THEMIS), and Magnetospheric Multiscale (MMS) have made it possible to study the deformations (ripples) of the shock surface. Due to the high cost of satellite missions, computer simulations are also used to study the features of particle acceleration. Simulations range from kinetic schemes, where each particle is followed, to fluid models, where the whole plasma population is approximated as a single fluid. Choosing the correct simulation method is essential for studying specific features of shock acceleration.

A Monte Carlo test particle simulation code is developed in this thesis to study the features of ripples in isolation. The key finding is that a quasi-parallel shock appears to be able to accelerate particles as efficiently as a quasi-perpendicular shock when the shock surface is fully rippled. The results indicate that the time the ripple is present at the shock surface determines the efficiency of the particle acceleration. The size of the ripple seems to define the maximum achievable acceleration.

The results highlight the importance of the deformation of the shock surface to particle acceleration. In the future, the results of these simulations should be compared with satellite observations and parameter combinations should be explored with the simulation code.

Keywords: space physics, particle acceleration, shock, ripple, simulation, Monte Carlo, test particle

TURUN YLIOPISTO
Fysiikan ja tähtitieteen laitos
SJÖBLOM, FRANS Hiukkaskiihdytysen simulointi epätasaisella plasmashokilla
Pro Gradu, 42 s.
Fysiikka
Toukokuu 2020
Turun yliopiston laatujärjestelmän mukaisesti tämän julkaisun alkuperäisyys on tarkastettu Turnitin Originality Check -järjestelmällä.

Plasmashokit pystyvät kiihdyttämään hiukkasia suuriin energioihin. Shokkigeometriasta riippuen hiukkasten energiaspektreissä on huomattavia eroja teorian ja havaintojen välillä. Viime aikoina modernit satellittihankkeet, kuten Cluster, Time History of Events and Macroscale Interactions during Substorms (THEMIS) ja Magnetospheric Multiscale (MMS), ovat mahdollistaneet shokkipinnan epätasaisuuden tutkimuksen. Satelliittien kalliin hinnan takia myös tietokonesimulaatiota käytetään plasman tutkimuksessa. Simulaatioiden skaalat vaihtelevat hyvin tarkoista kineettisistä malleista nestemalleihin. Kineettisissä simulaatioissa mallinnetaan tarkasti hiukkasten ratoja ja niiden vaikutusta sähkömagneettisiin kenttiin, kun taas nestemalleissa plasma yleistetään yhdeksi kollektiivisesti käyttäytyväksi nesteeksi. Shokkikiihdytyksen yksittäisten ominaisuuksien tutkimuksessa oikean simulaatiomenetelmän valinta on erityisen tärkeää.

Tutkielmassa kehitettiin Monte Carlo testipartikkelisimulaatio, jonka avulla pystyttiin yksitellen tutkimaan eri shokkipinnan epätasaisuuksien ominaisuuksien vaikutusta. Tutkielman tulokset antavat ymmärtää, että lähes pitkittäinen shokkipinta pystyy kiihdyttämään partikkeleita lähes poikittaisen shokin tyylisesti, kun pitkittäisen shokin pinta on täysin väreilevä. Tulokset osoittavat, että hiukkaskiihdytyksen tehokkuus määrittyy sen mukaan, kuinka usein pinta väreilee. Shokkipinnan väreilyn amplitudi vaikuttaa partikkelien suurimpaan mahdolliseen saavutettavaan energiaan.

Tulokset korostavat shokkipinnan väreilyn vaikutusta partikkelien kiihdytykseen. Jatkossa simulaatiotuloksia tulisi verrata havaintoihin ja simulaatiolla tulisi tutkia eri parametriyhdistelmien vaikutusta shokkikiihdytyseen.

Avainsanat: avaruusfysiikka, partikkelikiihdytys, shokki, väreily, simulaatio, Monte Carlo, testipartikkeli

Contents

Introduction

Plasma is one of the four common states of matter. Plasma is a gaseous fluid of ions with free electrons, but it is electrically neutral. Plasma is categorized as either weakly or fully ionized. The degree of ionization describes how much of the fluid is in a charged state as ions and electrons. Fully ionized plasma is a highly conductive fluid where long-range electric and magnetic fields direct the bulk behaviour of the matter. Most astrophysical plasmas are fully ionized.[Piel, 2017]

Space physics is an area of study that focuses on the plasma that occurs naturally in our solar system [Kallenrode, 2004]. The vast majority of plasma in interplanetary space is released from the Sun as solar wind, but there are particle populations originating from outside the solar system as accelerated particles known as cosmic rays. Shocks are one of the main sources of highly energetic particles in space.[Burgess and Scholer, 2015]

A shock is a sudden change in the flow speed of the medium bulk flow [Landau and Lifshitz, 1987]. The best example is the bow shock formed ahead of a jet plane flying faster than the sound speed in air. In space plasmas shocks are formed as blast waves in supernovae remnants, bow shocks in front of astronomical objects and as interfaces between different plasma flows in interplanetary space. Particles accelerated in shocks are seen from almost all astrophysical objects.[Kallenrode, 2004]

Near-Earth space is becoming increasingly important for modern human society with satellites, astronauts, and sensitive electrical equipment on Earth susceptible to changes in the surrounding space [Bothmer and Daglis, 2007]. The Earth is shielded from most charged particles from interplanetary space by its own magnetic field creating a layer known as the magnetosphere. The bow shock is formed ahead of the magnetosphere to slow down the solar wind plasma, which then flows around Earth in the magnetosheath.[Gombosi, 1998]

Fast moving plasma is slowed down in the bow shock, so it changes direction and flows around the magnetosphere. The properties of the solar wind are constantly changing, which in turn affects the magnetosphere and the rest of the near-Earth space.[Gombosi, 1998] To protect humans and sensitive equipment from the changing conditions (or space "weather"), it is important to understand the particle acceleration process in shocks [Bothmer and Daglis, 2007].

In-situ observations of near-Earth space are not an easy task. Satellites capable of observing and surviving in space require the expertise of multiple different fields of study and cost on average hundreds of millions of euros to build. Current satellite missions are collaborative works of multiple universities and governmental bodies.[Wertz and Larson, 1999]

Computer simulations offer a different avenue for studying space physics. Simulations in plasma physics are divided to kinetic and fluid models. Fluid models approximate the plasma as one or more interacting bodies of fluid and kinetic models rely on solving kinetic (Vlasov) and Maxwell equations for all particles in the simulation. Kinetic models are more accurate in their description, but are more computationally expensive. Hybrid models combine the kinetic approach for ions with the fluid description for electrons [Winske and Omidi, 1996; Birdsall and Langdon, 2018; Palmroth et al., 2018].

In Figure 1 is the result of a hybrid simulation from the Vlasiator team at the University of Helsinki. It shows a snapshot of plasma density in near-Earth space, where blue is lower and red is higher plasma density. Comparing the IMF and bow shock normal direction splits the bow shock into the quasi-parallel and quasi-perpendicular regions. The quasi-perpendicular region is smooth compared to the deformed quasi-parallel region of the bow shock.

Simulation results only work in tandem with observations and there is a difference when comparing the particle energy spectra of simulations and observations. Some of

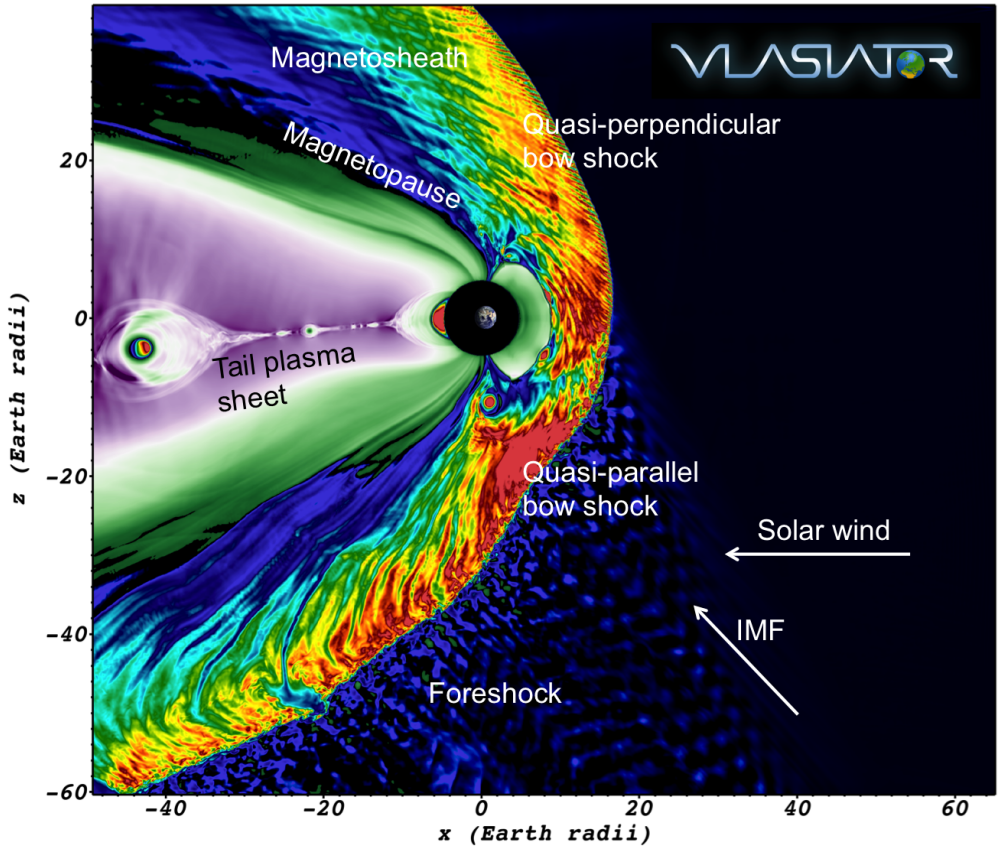

Figure 1. A snapshot of Earth's bow shock and related areas from a Vlasiator hybrid-Vlasov simulation. The figure is from Palmroth et al. [2018].

these differences are due to the finite timestep and size of the simulation.[Birdsall and Langdon, 2018] Recently many studies on the difference in particle acceleration have focused on the approximation of a planar and smooth shock surface [e.g., Gingell et al., 2017; Páez et al., 2019]. Simulations such as the Vlasiator have shown that the shock surface is rippled, but the rippling of the shock is always present in this type of simulations and thus these simulations struggle to discuss the importance of the rippling to particle acceleration. With this thesis the goal was to develop a simulation code capable of isolating the effects of the ripple and use it to begin to explore changes in particle acceleration by adding a controlled ripple to a smooth shock surface.

This thesis is organized as follows. Chapter 1 introduces the background of

plasma shock physics and particle acceleration. Chapter 2 discusses different simulation methods in plasma physics and why a Monte Carlo test particle simulation was chosen for this thesis. Chapter 3 focuses on the development of the simulation code and explains in detail the model and functions the simulation code uses. Chapter 4 introduces the results of the thesis and Chapter 5 discusses the results. Finally in Chapter 6 a brief conclusion is followed by consideration of possible future work. Also the two Appendices have detailed derivations of how the rippled surface is simulated (Appendix A) and how the limited acceleration time of the simulation affects the results (Appendix B).

1 Space physics and shocks

1.1 Shocks in plasma

A shock is a thin moving interface between two fluid populations, where the flow of the fluid changes from supersonic to subsonic. Shocks in plasma are commonly modeled with magnetohydrodynamics (MHD). MHD is a fluid model of plasma where the hydrodynamic equations are expanded with the inclusion of electromagnetic properties of the particles. The equations that govern the flow in the ideal case of magnetized conducting fluids are [Burgess and Scholer, 2015]:

$$\frac{\partial \rho}{\partial t} + \nabla \cdot (\rho \boldsymbol{V}) = 0 \tag{1}$$

$$\frac{\partial}{\partial t}(\rho \boldsymbol{V}) + \nabla \cdot \left[\rho \boldsymbol{V}\boldsymbol{V} + \left(p + \frac{B^2}{2\mu_0}\right)\boldsymbol{I} - \frac{\boldsymbol{B}\boldsymbol{B}}{\mu_0}\right] = 0 \tag{2}$$

$$\begin{aligned}\frac{\partial}{\partial t}\left(\frac{\rho V^2}{2} + \frac{p}{\gamma - 1} + \frac{B^2}{2\mu_0}\right) + \\ \nabla \cdot \left[\left(\frac{\rho V^2}{2} + \frac{\gamma}{\gamma - 1}p + B^2\right)\boldsymbol{V} - (\boldsymbol{V} \cdot \boldsymbol{B})\boldsymbol{B}\right] = 0\end{aligned} \tag{3}$$

$$\frac{\partial \boldsymbol{B}}{\partial t} + \nabla \cdot (\boldsymbol{V}\boldsymbol{B} - \boldsymbol{B}\boldsymbol{V}) = 0 \tag{4}$$

$$\nabla \cdot \boldsymbol{B} = 0, \tag{5}$$

where ρ is density, $\boldsymbol{V}$ is plasma velocity, p is pressure, $\boldsymbol{B}$ is magnetic field, μ_0 is magnetic permeability, $\boldsymbol{I}$ is identity matrix and γ is specific heat ratio. Equations (1)-(4) are the conservation of mass, momentum, energy and magnetic flux and Equation (5) is the zero divergence condition. Together Equations (1)-(5) are called the shock conservation relations, the shock jump conditions or the MHD Rankine-Hugoniot relations.[Burgess and Scholer, 2015]

Solving Equations (1)-(5) leads to four different types of discontinuities: The first three are the contact and tangential discontinuities, where the mass flow between

the plasma populations is zero, and the rotational discontinuity, where the pressure difference between the two plasma is zero. Finally, the discontinuity where both the mass flow and density changes, is called a shock. Shocks can be divided further to fast, intermediate and slow shocks by the upstream plasma flow speed.[Burgess and Scholer, 2015]

The shock is not just a discontinuity, but has a small chaotic structure inside the transition between upstream and downstream. The transition layer is dominated by small instabilities in the electric and magnetic field. The transition layer has a negligible effect on the acceleration of particles and there are very little measurements of the actual transition layer in a plasma shock in space.[Gary and Gary, 1993] Shocks move at such high speeds that the transition layer can only be seen with instruments that have the ability to take measurements at least several times a second. One satellite mission capable of such high frequency observations is the Magnetospheric Multiscale (MMS) mission [Baker et al., 2016]. Such measurements are usually only done with magnetic field instruments and other instruments take measurements once a second at the fastest. For example, for the plasma instruments that measure the velocity of particles, the shock appears as a discontinuity.[Burgess and Scholer, 2015]

Wave speeds are anisotropic in magnetohydrodynamics. Thus the magnetic field geometry at the shock and the angle of incidence become very important. The parameter defining this geometry at the shock is the shock normal angle $\theta_{B\boldsymbol{n}}$. Since the shock normal angle plays such a key role in defining the magnetohydrodynamic shock, it is used to divide the shocks into different categories: the parallel shock $\theta_{B\boldsymbol{n}} = 0$, the quasi-parallel shock $\theta_{B\boldsymbol{n}} < 45°$, the quasi-perpendicular shock $\theta_{B\boldsymbol{n}} > 45°$ and the perpendicular shock $\theta_{B\boldsymbol{n}} = 90°$. The division between a quasi-perpendicular and quasi-parallel shocks is just an agreed upon convention and not based on any clear difference in the shocks. Sometimes oblique is used to characterize all shocks

with the shock normal angle between $0° < \theta_{B\boldsymbol{n}} < 90°$.[Burgess and Scholer, 2015]

Since shocks are described by the shock speed and plasma properties in the upstream and downstream, the choice of coordinate frame is very important. There are a lot of different choices for the coordinate frame in space research (Heliocentric, geocentric, shock centered, etc.). With shock simulations there are two main coordinate frames used: the normal incidence frame (NIF) and the de Hoffmann-Teller frame (HTF) [Ellison, 1981]. With discontinuous shocks there are three main velocities that describe the system: the shock propagation, bulk upstream and downstream velocities. If we study only non-relativistic shocks, particle positions and velocities can be calculated between any two frames using the Galilean transformation. Galilean transformation doesn't change the magnetic field at all, but the electric field has an added term from the movement of the fields

$$\boldsymbol{B}' = \boldsymbol{B} \tag{6}$$

$$\boldsymbol{E}' = \boldsymbol{E} + \boldsymbol{v}_{ff} \times \boldsymbol{B}, \tag{7}$$

where unprimed electric and magnetic fields are from the first frame, primed are the second frame and $\boldsymbol{v}_{ff}$ is the velocity of the first frame relative to the second.[Burgess and Scholer, 2015]

The normal incidence frame is fixed to the shock and has the upstream plasma flow directed along the shock surface normal vector. As we will see later, the normal incidence frame is insufficient when studying the effects of ripples in shocks. Using a Galilean transformation one can find a frame where the upstream flow and magnetic field are aligned so that the electric field becomes zero. This frame that has no electric field is called the de Hoffmann-Teller frame. The velocity change from normal incidence frame to de Hoffmann-Teller frame is called the de Hoffmann-Teller velocity, $\boldsymbol{v}_{HT}$, and the velocity required for the change can be calculated using the shock normal angle and upstream plasma velocity

$$\boldsymbol{v}_{HT} = \boldsymbol{V}_u \tan\theta_{B\boldsymbol{n}}. \tag{8}$$

As the shock normal angle approaches 90° the de Hoffmann-Teller velocity increases so rapidly that relativistic transformations are needed. Particle motion near the shock is easier to describe in the de Hoffmann-Teller frame since in there is no $\boldsymbol{E} \times \boldsymbol{B}$ drift.[De Hoffmann and Teller, 1950]

The mean free path of particles is much larger in plasma than in ordinary gas dynamics [Burgess and Scholer, 2015]. Because of this the energy dissipation mechanism of MHD shocks must be different from the binary collisions that dissipate the energy in hydrodynamic shocks. In-situ observations of Earth's bow shock revealed that the dissipation mechanism in plasma shocks is particle deflection and acceleration [Scudder et al., 1986a,b,c]. Since the energy dissipation of the total population of incoming plasma is achieved by accelerating a small fraction of the particles, the dissipation mechanism cannot be explained with ordinary hydrodynamic equations. The particle acceleration of plasma shocks can be further be divided into two distinct groups according to the magnetic field geometry at the shock: the quasi-perpendicular and the quasi-parallel.

In observations these regions are very distinct with the perpendicular region being a clear discontinuous jump from otherwise smooth upstream and downstream and the parallel region being a irregular region both upstream and downstream of the shock. In collisionless shocks a fraction of upstream ions are reflected at the shock. These backstreaming ions gyrate around the magnetic field and the motional electric field accelerates them. In quasi-perpendicular geometry the accelerated ions return to the shock quickly. In quasi-parallel geometry the backstreaming ions can escape far upstream and excite waves in the plasma which in turn scatter the particles away from the magnetic field direction. This leads to a complex feedback network that is not well defined.[Burgess and Scholer, 2015] The Cluster mission

found in observations of the quasi-parallel region that even four satellites is too few to properly analyze the evolution of the irregularities [Lucek et al., 2008].

1.2 Diffusive Shock Acceleration

Multiple independent studies published in 1977 and 1978 showed that a moving shock was able to accelerate some of the particles that are diffusing in the plasma. This acceleration process relies on the scattering of the accelerated particles at both sides of the shock. The analytical derivation of the diffusive shock acceleration shows that the momentum particle gains is proportional to the momentum it already has and the probability of the particle escaping from the shock. Both of these factors are determined by the ratio between plasma velocity along the shock normal upstream and downstream. The ratio between these velocities is also known as the gas (or shock) compression ratio.[Axford et al., 1977; Krymskii, 1977; Bell, 1978a,b; Blandford and Ostriker, 1978]

Figure 2 shows a simplified explanation how a particle is accelerated in a parallel shock with diffusive shock acceleration. Particle velocity can be divided to the parallel ($\boldsymbol{v}_{\parallel}$) and perpendicular ($\boldsymbol{v}_{\perp}$) velocities. We consider the magnetic fluctuations, which scatter the particles, to be frozen-in to the upstream and downstream plasma flows. In this case, when considering the scattering process anywhere in the two plasma frames, the total energy of the particle is conserved. This means that the velocity vector magnitude is conserved and only the magnitudes of the components can change. Thus a particle moving in the upstream or downstream can only have velocities on the half circle with the origin at u_1 or u_2. The center points for the circles are the upstream (u_1) and downstream (u_2) plasma flow speeds. In the Figure the numbered points signify shock crossings with $\boldsymbol{v}_{\parallel} > 0$ the particle moving in the downstream direction and $\boldsymbol{v}_{\parallel} < 0$ the upstream direction. With each shock crossing the particle can only change to the other plasma flow speed half circle and thus

gains energy in the form of perpendicular velocity. As the shock crossings continue to happen and the half circles get larger the probability of the particle to scatter back to the upstream direction gets closer to 50%.[Sugiyama and Terasawa, 1999]

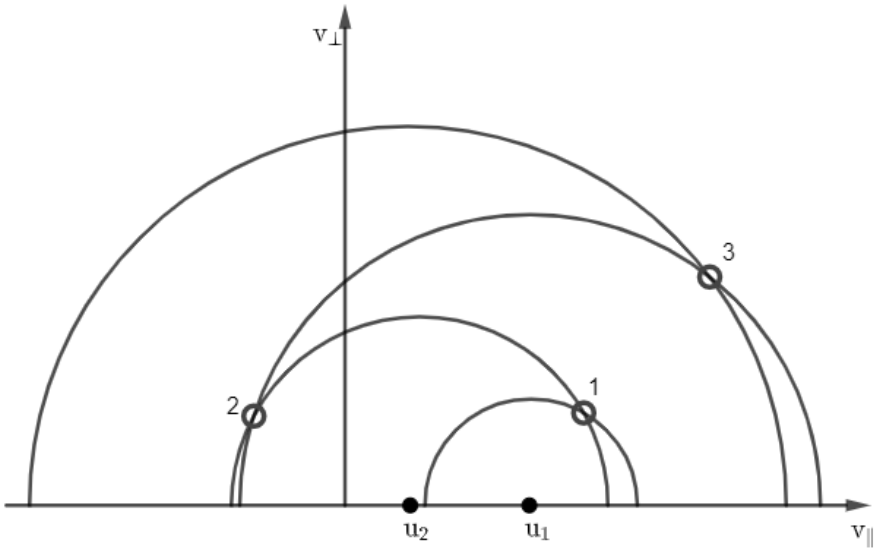

Figure 2. Example of how a particle can accelerate with diffusive shock acceleration. Particle velocities are divided to parallel ($v_\parallel$) and perpendicular ($v_\perp$). Possible particle velocities are depicted as half circles around the upstream (u_1) and downstream (u_2) plasma flow speeds. Shock crossings happen at numbered points 1, 2 and 3. The Figure is adapted from Sugiyama and Terasawa [1999].

The downstream particle velocity spectrum that results from the diffusive shock acceleration is

$$\frac{\mathrm{d}N}{\mathrm{d}v} = \frac{3N_0}{(r-1)v_0}\left(\frac{v}{v_0}\right)^{-\gamma}, \tag{9}$$

where N is the number of particles, N_0 is the number of particles injected into the acceleration process, v is the velocity of the particle, v_0 is the starting velocity of the particles, r is the gas compression ratio and $\gamma = (r+2)/(r-1)$.

The analytical derivation of the diffusive shock acceleration assumes an infinite planar shock and that the upstream and downstream continue to infinity on their

respective sides of the shock. In nature this is clearly not true and the acceleration time of particles is limited [Forman and Morfill, 1979]. Due to the limited acceleration time there is a maximum velocity the particles can be accelerated to, after which the power law no longer matches observations [Vainio, 1999]. The analysis of the simulation results in this thesis uses a modified version of the Vainio [1999] calculation of the maximum (cutoff) velocity particles can attain with limited simulation time. The derivation of the cutoff velocity is done in Appendix B.

1.3 Rippled shock

The shock surface is not smooth [Winske and Quest, 1988; Bale et al., 1999]. Significant discrepancies between observations and theory have been noted when, for example, the energy spectrum and local density jump at the shock has been compared in single spacecraft measurements. The addition of turbulence to the shock surface is able to partly explain such differences in theory and observations.[Giacalone and Neugebauer, 2008]

Deformations of the shock surface can be further divided into subcategories of corrugations and ripples. Ripples are small scale fluctuations in the magnitude of ion gyroradius and corrugations are large scale fluctuations that permeate through the whole shock surface.[Johlander et al., 2016; Páez et al., 2019] Similar to the division between perpendicular and parallel shocks, the difference between ripples and corrugations is just a convention and does not imply any significant differences between them. Corrugated features have been used to explain the differences with theory and observation of coronal mass ejection driven shocks [Páez et al., 2019]. Susino et al. [2015] proposed that corrugated shape of the shock surface does not change from the initial irregularities.

Ripples were first discovered in an hybrid simulation of quasi-perpendicular shock [Winske and Quest, 1988]. Using Fourier transforms, analysis of quasi-perpendicular

simulations found that the power spectrum has a maximum at a wavelength of several ion inertial lengths [Lowe and Burgess, 2003]. As seen in Figure 1 the bow shock quasi-perpendicular region is much smoother than the quasi-parallel region. The rippling of the shock surface has been used to explain areas of enhanced plasma flow downstream of the quasi-parallel shock. Modeling a controlled ripple Hietala and Plaschke [2013] found that a bow shock ripple with amplitude to wavelength ratio of 0.09 that was present 12% of the total simulation time, was able to explain almost all of the deviations of the plasma flow.

The in-situ observation of ripples in the parallel region require multipoint spacecraft data with distances near the ion gyroradius. Published in-situ observations of these ripples have begun only recently with space missions such as, Cluster, Time History of Events and Macroscale Interactions during Substorms (THEMIS) and Magnetospheric Multiscale (MMS) mission. With observational results, ripples have been confirmed to be periodic and propagating deviations to the average shock angle. Currently there are no widely agreed upon explanation for the rise of these disturbances.[Gingell et al., 2017]

Since the acceleration of particles in plasma shocks is mainly dependent on the plasma density difference across the shock and the shock surface is deformed, the observed particle energy spectrum should be different depending on the measurement point. Analysis of single spacecraft observations has revealed significant differences in the low energy (100 keV) particle fluxes [Neugebauer and Giacaione, 2005]: Two spacecraft observations showed that when ripples are larger than the separation of the spacecraft, the particle energy spectra downstream of the shock is determined by the average density difference across the shock. Figure 3 shows a single-fluid MHD simulation used by Giacalone and Neugebauer [2008] to confirm their observations of different gas compression ratios from the same shock. They simulated the plasma shock by injecting the plasma from the left hand side and having a rigid wall at the

right hand side. This formed a plasma pileup at the right hand side which formed a shock that travelled back to the left hand side. The Figure shows upstream as lighter and downstream as darker gray. The dotted lines a and b are where plasma densities and particle spectra are computed and compared.

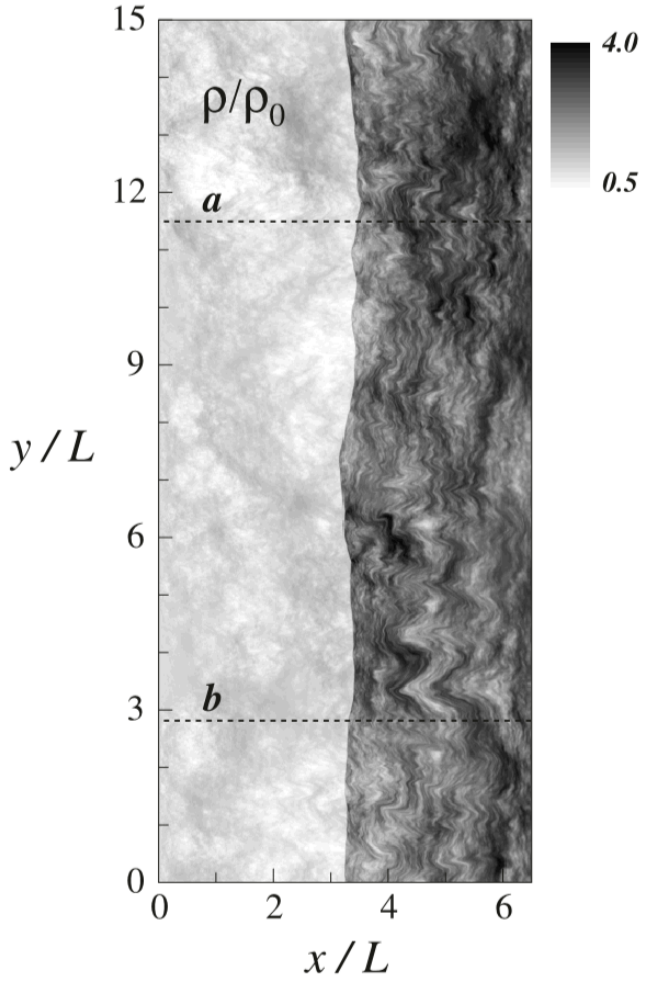

Figure 3. A single-fluid MHD simulation used to study the ripples effect on multiple spacecraft observations. The lighter gray represents upstream and the darker gray downstream. The dotted lines a and b are where the simulated observations are made. Credit: Giacalone and Neugebauer [2008]

The MMS mission has been successfully used to identify a rippled shock at the ion inertial length scale. The Figure 4 shows a reconstruction done by Johlander et al. [2016] for a shock transition by MMS on October 7, 2017, 11:44 UT. The transition from upstream to downstream was accompanied by multiple shifts in the

plasma measurements, which was explained with a rippled shock. Finally, MMS mission observations have shown that the movement of the ripples are important and any steady state simulation with ripples estimates particle acceleration incorrectly.[Gingell et al., 2017]

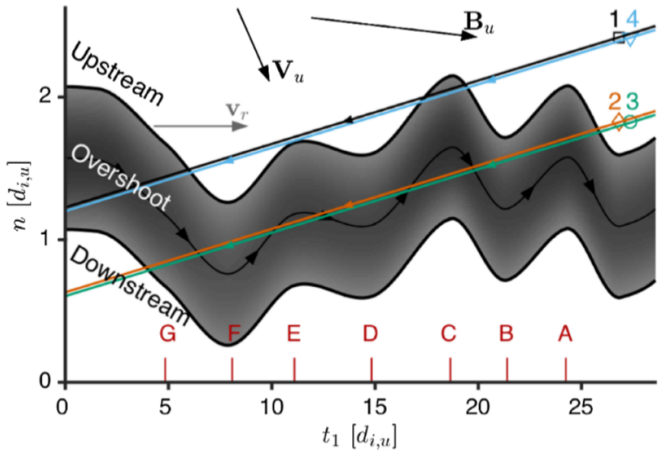

Figure 4. Reconstruction of a shock crossing by MMS. The colored lines are the four spacecraft. Credit: Johlander et al. [2016]

Clearly the effects of ripples must be studied in detail. Currently published simulations mainly use 2 dimensional or 2.5 dimensional hybrid-PIC or hybrid-Vlasov description, which are very accurate in their description of plasma physics. But the down side is that these simulations do not have control over the ripple and thus ripples can not be studied in isolation. The goal of this thesis is to develop a tool to study the important parameters of ripples using a more simple simulation, but having full control over the ripple to see how each parameter contributes to particle acceleration.

2 Simulations in space physics

Statistical physics uses mathematical tools to study large ensembles and approximations to solve physical problems. More specifically statistical mechanics use the microscopic properties of individual particles to study the macroscopic properties of fluids and solids.[Huang, 2009] Unfortunately only a fraction of non-trivial problems in statistical physics have an exact solution with the two-dimensional Ising model being a famous example. Some problems in statistical physics have solutions following simple approximations. For liquids however, there are usually no simple approximations that do not alter the way the theoretical model mimics a real liquid.[Allen and Tildesley, 2017]

Computer simulations of plasma physics can be divided into groups. Before discussing different simulation schemes the first question is whether the simulation is self-consistent or not. If a simulation is self-consistent that means that the movement of the particles affects the electric and magnetic field of the bulk plasma. Self-consistent simulations are more accurate, but are also require more calculations to run.[Winske and Omidi, 1996]

The most accurate simulation scheme in plasma physics is the so called particle-in-cell (PIC) simulation. This is a self-consistent simulation where the particle movement is calculated on a grid [Morse and Nielson, 1969]. At each timestep each particles effect on the electric and magnetic field is divided to the four closest grid points and then the total effect of the four closest grid points is used to calculate the trajectory of each particle.[Birdsall and Langdon, 2018] Even though only 1 % of the total population of particles need to be ionized to turn gas into plasma this still means millions of particles effect to the EM-fields need to be calculated. For this reason PIC simulations are only used to simulate small and/or short phenomena in plasma physics.[Winske and Omidi, 1996]

The next scheme is best known as the Vlasov simulation, but has also been called

the continuum method. This is where instead of following single particles the simulation relies on particle distributions and continually solves the Vlasov and/or Poisson equation to trace the particle trajectories. There are many implementations of the Vlasov method (Semi-Lagrangian, Fourier transform and Finite-Difference methods to name a few).[Palmroth et al., 2018] The Vlasov method can be self-consistent or not depending on whether the electric and magnetic fields are calculated using Maxwell's equations or if the fields are static [Büchner, 2005].

The PIC and Vlasov methods employ classical mechanics to follow particles in simulations. The following methods use the collective properties of the particles in plasma to make use of hydrodynamics. The next method is known as the two-fluid plasma model and uses the hydrodynamic equations to track separately the ions and electrons in plasma. The electric and magnetic fields are described using Maxwell's equations.[Krishan, 1999] The two-fluid model can also be mixed with PIC or Vlasov method to use so called hybrid schemes where electrons are considered a fluid but ions are calculated in either of the more accurate methods. One example of a hybrid method is the Vlasiator project where ions are considered as a velocity distribution function and electrons are a fluid.[Palmroth et al., 2018]

The next method is the magnetohydrodynamic fluid model where plasma is considered as a single fluid. Usually in a MHD simulations the ions are still described by the full set of Euler equations, but electons are neglected with approximations of infinite light speed, quasi-neutrality and massless electrons. The assumption of infinite light speed unfortunately gives a way for wave speeds that grow without bound and artificial diffusivity has to be added to the simulation.[Birdsall and Langdon, 2018]

Finally the method used in this thesis is the test particle method. In this system the kinetics of bulk plasma flow and the electric and magnetic fields are fixed. A single particle, the so called test particle, is released in the system and is then

followed. The test particle is assumed to have no effect on the overall system and thus no effects to the bulk plasma or EM-fields are considered.[Birdsall and Langdon, 2018]

In this thesis the test particle method is combined with the Monte Carlo general simulation method. The Monte Carlo method tries to find approximate solutions to problems by using repeated random sampling. The Monte Carlo test particle method solves the steady-state Boltzmann equation numerically [Ellison, 1981]. The Monte Carlo test particle method is both simple to implement and computationally very widely applicable. While testing, the simulation can be run with only a small sample of particles, which makes it very fast to test, and the final simulations can be run with large sample of particles, which reduces noise in the final results.[Allen and Tildesley, 2017]

3 Monte Carlo test particle simulation of particle acceleration with rippled shocks

3.1 Development of the code

The implementation of the code started with testing the Monte Carlo simulation method. The first test was with a random walk simulation where a particle on a two dimensional plane had four choices of movement of equal probability. At each step the particle was assigned randomly either up, down, left or right as a direction and then it was moved a predefined length in that direction.

The next iteration of the code followed a particle in large scale magnetic fields. Here particle movement is governed by two differential equations:

$$\frac{dz}{dt} = \mu V$$
$$\frac{d\mu}{dt} = \frac{1-\mu^2}{2L},$$

where z is the position, V is the velocity and μ is the pitch-angle cosine of the particle and t is the time and L is the length scale of the magnetic field. Solving z and μ using a small time step δt gives

$$z = z_0 + \mu_0 V \delta t$$
$$\mu = \mu_0 + \frac{1-\mu^2}{2L(z_0)} V \delta t.$$

There is no electric field so the velocity of the particle does not change and the particle is moving with constant speed.

Charged particles in electromagnetic fields follow a helical motion. The radius of the rotational movement is called the Larmor radius (or gyroradius). If the magnetic field varies in a much larger scale than the particle gyrates, then we can use the so

called guiding center approximation. Instead of following the true motion of the particle, we follow the center point of the gyration. In a homogeneous field, the guiding center just follows the magnetic field. If there is small variation in the magnetic field, the energy conservation is contained in the magnetic moment of the particle. The guiding center approximation allows the simulation to take much larger timesteps. If we want to simulate particle acceleration in shocks using the Monte Carlo method having the timestep as big as possible keeps the simulation times small. Unfortunately using the guiding center approximation doesn't allow us to study the effect of the transition layer of the shock and we approximate the shock as a discontinuity of infinitesimal thickness.[Burgess and Scholer, 2015]

After successfully implementing a code that follows a particle in a magnetic field the next step was to add a shock in the physical system. Before moving the particle the code observes whether the particle is in the upstream ($x < 0$) or downstream ($x \geq 0$). The upstream plasma speed stayed as a user parameter and the downstream plasma speed was calculated using the gas compression ratio. The shock is modeled as a MHD shock. When moving the particle, if the particle would move from one side to the other, the code checks if the particle is transmitted or mirrored at the shock. The parameters the user can control for the shock are: the shock normal angle $\Theta_{B_{<n>}}$ and gas and magnetic field compression ratios r_g and r_B.

In the code it is convenient to compute the particle propagation in the shock rest frame, but scatter in relation to the bulk plasma flow. This is because we consider the magnetic irregularities scattering the particle to be frozen into the bulk plasma flow. This is also known as the so-called magnetostatic approximation.[Ellison, 1981] Easiest way to implement that was to add a function `changeFrame` that would change the particle velocity and pitch angle between the shock frame and the bulk plasma flow frame. The frame change happens with a Galilean transformation and that means that the code will not be able to accurately track relativistic particles.

In the end a decision was made that the simplicity of a Galilean transformation outweighed the added usability of tracking relativistic particles.

After adding a shock to the simulation the next step was to randomize the start time of each particle. This has the physical meaning of having a constant injection of particles like in shocks in the interplanetary space or the Earth's bow shock. In the old versions of the code, all the particles had the same release time which meant physically having an instantaneous release.

Next addition to the code was the obliquity of the shock. Instead of only having a parallel shock the simulation needed to allow for a range of angles between the plasma flow and shock normal. To add the effect of obliquity the simulation needed to take into account also the change in the magnetic field at the shock. Also with oblique shocks there is a possibility that the particle does not go through the shock and mirrors at the shock.

The last major addition to the simulation was the added complexity of the ripple. The ripple was modeled as a sinusoidal surface

$$f(x, y, z) = z - A \sin kx \sin ky, \tag{10}$$

where A is the ripple amplitude, $k = \frac{2\pi}{\lambda_{wl}}$ is the wavenumber of the ripple and λ_{wl} is the wavelength of the ripple. Taking the unit vector of the magnetic field in the upstream, $\boldsymbol{b}$, and calculating the surface normal at a random point, $\boldsymbol{n}$, gives the shock normal as

$$\cos \Theta_{Bn} = \boldsymbol{n} \cdot \boldsymbol{b} = \frac{\cos \Theta_{B<\boldsymbol{n}>} - a \sin \Theta_{B<\boldsymbol{n}>} \cos 2\pi x \sin 2\pi y}{\sqrt{a^2(\cos 2\pi x^2 \sin 2\pi y^2 + \sin 2\pi x^2 \cos 2\pi y^2) + 1}}, \tag{11}$$

where Θ_{Bn} is the shock normal angle at a random point, $\Theta_{B<\boldsymbol{n}>}$ is the average shock normal angle, x and y are random points on the surface and $a = 2\pi A/\lambda_{wl}$, where A is the ripple amplitude and λ_{wl} is the ripple wavelength. Figure 5 shows a cross-section of different rippled surfaces. The complete derivation of the modeled

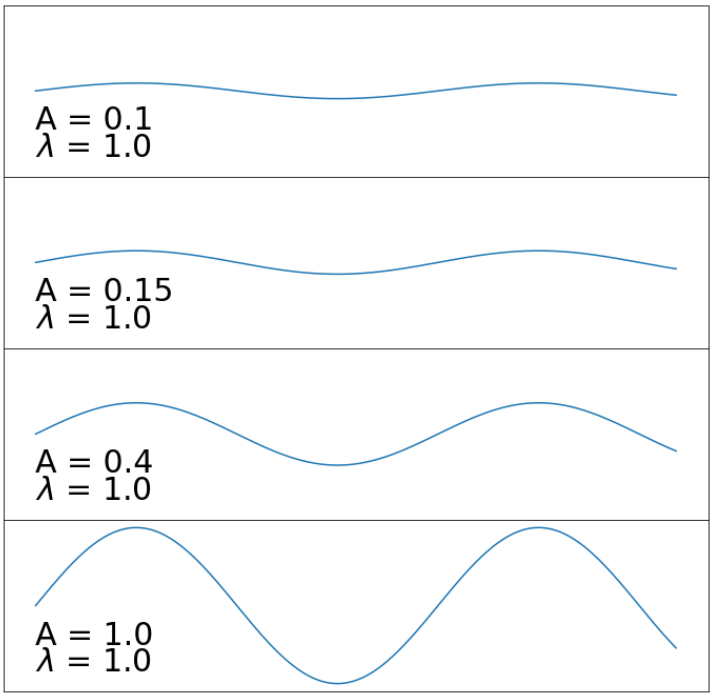

Figure 5. Examples of different ripples.

ripple is in Appendix A.

The user is prevented from choosing parameters that generate ripples that lead to 90° or larger angles between the plasma flow and shock normal, because of the frame changes between the near incidence and de Hoffmann-Teller frames. Now each time a particle is crossing the rippled shock from upstream to downstream the simulation calculates the obliquity of the shock from the user defined ripple surface. The user also has control over the probability of the particle crossing the rippled or non-rippled shock surface as it is a simulation parameter. There might be for example situations where there are multiple smaller ripples moving on the shock surface.

3.2 Overview of the code

All particles are injected to the upstream side of the shock with the same speed and random starting direction. In this simulation the scattering is approximated by calculating a random walk style solution. The scattering must be done in the plasma frame so the frame of reference must be changed from the de Hoffmann-Teller to the normal incidence frame and back at each timestep.

If during the timestep the particle crosses the shock the simulation will first decide whether a ripple is present or not based on the user parameters. If the particle is crossing a rippled shock then a new frame change is needed so that the particles are in the normal incidence frame of the rippled surface. The shock crossing is calculated assuming that the magnetic moment (first adiabatic invariant) of a particle remains constant. Using the adiabatic invariant the simulation can calculate whether the particle is mirrored or transmitted through the shock.

After particle movement in the normal incidence frame the length of the next timestep is calculated using the particle speed. This ensures that the particle does not move large distances during one timestep, even if it has accelerated to a large velocity. The simulation ends when the total time of the timesteps exceeds the simulation time, which is a user parameter.

The code is divided into three files: `rippled_shock.py` , `simulation_functions.py` and `simulation_parameters.py` . The parameters file only consists of the changeable simulation parameters called by the main simulation file `rippled_shock.py` and contains no actual code. The parameters allow the user to have full control over the plasma, shock and most importantly the ripple itself.

The files `rippled_shock.py` and `simulation_functions.py` contain the following functions:

changeFrame. *Calculates the new velocity and pitch-angle cosine for a particle when the frame of reference is changed. The simulation uses Galilean transformation*

so the equations are

$$v_2 = \sqrt{(v_1\mu_1 - u)^2 + v_1^2(1-\mu_1^2)} \tag{12}$$

$$\mu_2 = \frac{v_1\mu_1 - u}{v_2}, \tag{13}$$

where v is velocity, μ is pitch-angle cosine, u is bulk plasma velocity and 1 indicates the old frame and 2 the new frame.

scatterParticle. *Calculates new pitch angle for a particle using two random numbers simulating scattering in plasma.*

$$\theta = \sqrt{-2\delta t v \log(1-R_1)} \tag{14}$$

$$\phi = 2\pi R_2, \tag{15}$$

where δt is the length of the timestep, v is the particle velocity and $R_{1,2}$ are random numbers from the half open interval [0,1). Using θ and ϕ the new pitch angle can be calculated with

$$\mu_{new} = \mu_{old}\cos\theta + \sqrt{1-\mu_{old}^2}\sin\theta\cos\phi. \tag{16}$$

calculateRippleX. *Calculates shock ripple x-position using Equation (26) from the Appendix A. The x-position is solved iteratively from*

$$x_{n+1} = x_0 + A\tan\Theta_{B_{<\boldsymbol{n}>}}\sin 2\pi y_0 \sin 2\pi x_n \tag{17}$$

$$x_0 = x_0, \tag{18}$$

where A is the ripple amplitude, $\Theta_{B_{<\boldsymbol{n}>}}$ is the mean obliquity of the shock and y_0 and x_0 are random variables between the half open interval of [0,1). The calculation stops after there is no difference up to six decimals between the two most recent iterations. An accuracy of six decimals was chosen to be accurate enough for the simulation but fast enough to not slow the simulation significantly.

calculateCompressionRatios. *Calculates shock magnetic compression ratio and the movement speed of the ripple. Using the x-position calculated with* `calculateRippleX`

and the same random y-position the magnetic compression ratio of the shock can be calculated using

$$\cos\Theta_{B\boldsymbol{n}} = \frac{\cos\Theta_{B_{<\boldsymbol{n}>}} - a\sin\Theta_{B_{<\boldsymbol{n}>}}\cos 2\pi x \sin 2\pi y}{\sqrt{a^2(\cos^2 2\pi x \sin^2 2\pi y + \sin^2 2\pi x \cos^2 2\pi y) + 1}} \tag{19}$$

$$r_B = \frac{\sqrt{1 + r^2\tan^2\Theta_{B\boldsymbol{n}}}}{\sqrt{1+\tan^2\Theta_{B\boldsymbol{n}}}}, \tag{20}$$

where r_B is the magnetic compression ratio, r is the gas compression ratio, $\Theta_{B\boldsymbol{n}}$ is the situational obliquity of the shock and $a = 2\pi A/\lambda_{wl}$, where A is the ripple amplitude and λ_{wl} is the ripple wavelength.

Also the function calculates the movement speed of the ripple using

$$\delta u = \frac{a(\boldsymbol{V}_x \cos 2\pi x \sin 2\pi y + \boldsymbol{V}_y \sin 2\pi x \cos 2\pi y}{a\sin\Theta_{B_{<\boldsymbol{n}>}}\cos 2\pi x \sin 2\pi y - \cos\Theta_{B_{<\boldsymbol{n}>}}}, \tag{21}$$

where $\boldsymbol{V}_x$ and $\boldsymbol{V}_y$ are the ripple velocity in x- and y-direction and other variables are the same as in calculating the magnetic compression ratio.

moveParticle. *Moves the particle in relation to the shock. If the particle would cross the shock from the upstream side then the function changes the frame of reference to the rippled shock frame. After the frame change the code checks whether the particle is transmitted through or reflected at the shock using the fact that the adiabatic invariant stays constant. The particle is transmitted through the shock if*

$$\mu > \sqrt{1 - \frac{1}{r_B}}, \tag{22}$$

where μ is the pitch-angle cosine and r_B is the magnetic compression ratio.

Finally the frame of reference is changed back to the stationary shock frame. If the particle crosses the shock from downstream to upstream there is no possibility of reflection so it is transmitted through the shock.

simulateParticle. *Runs the simulation for a single particle using the previous functions. Before starting fixes the random seed in the simulation. Simulates particle movement using the following steps:*

1. *Check if the particle is upstream or downstream*
2. *Change from shock frame to plasma frame*
3. *Calculate new timestep using particle velocity*
4. *Scatter the particle*
5. *Change from plasma frame to shock frame*
6. *Check if the shock is rippled*
7. *Move particle*
8. *Add timestep to time*
9. *If time has not reached total simulation time go back to start*
10. *Return final info (particle number, position, velocity, μ)*

parallelSim. *Creates a list of particles to simulate from user defined parameters and parallelize the simulation to use all available cores on the machine. The starting parameters are all defined by the user except the pitch angle and starting time of each particle. The pitch angle is random between (-0.5,0.5) and the starting time is random between zero and total simulation time.*

The parallelization of the code is implemented using Python library multiprocessing. The library has specifically been adapted to parallelizise functions with multiple input values.

writeResult. *Updates a list of results with each particle in the simulation. Is a separate function to safeguard the list from* `parallelSim` *function writing multiple results to the list at the same time.*

3.3 Data processing

The result of each simulation is saved as list of each particle's number and its final position, velocity, cosine of pitch angle and simulation time. To compare the results of the simulation to the power law equation (9) all upstream particles need to be dropped. This removes in general around 6-8% of the total particle population. The

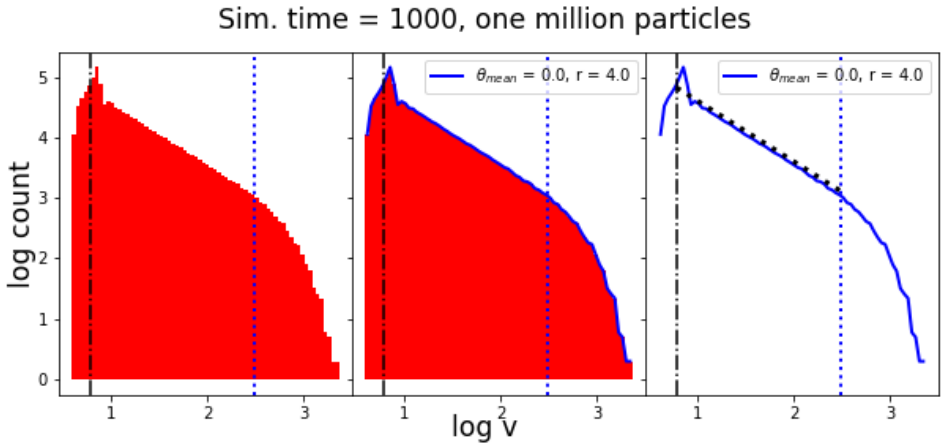

Figure 6. A three Figure series showing how particle energy spectra results are drawn. The dash-dotted vertical line is particle starting velocity and the blue dotted vertical line is the cutoff velocity (24). In the final panel a power law is drawn for comparison using the Equation (9).

results are presented in a log-log plot for better comparison, since then the power law is linear

$$\log \frac{dN}{d \log v} = \log C + (1 - \gamma) \log v, \tag{23}$$

where C is a constant containing all constants from Equation (9).

The next step in data processing is to calculate the logarithm of velocity for each particle. After that the particles need to be counted in a histogram of the logarithm of the velocity. The number of bins (cf. energy channels in plasma instruments) in the histogram can be chosen freely, but the results are more irregular the more bins are chosen. In this thesis the results are calculated with 70 bins. In Figure 6 this is done in the left panel. In the center panel a line plot is made using the top center point of each bin. Finally the histograms are removed and the power law is drawn for comparison using Equation (23).

Also to the results are drawn the starting velocity of the particles in the simulation as a dash-dotted black vertical line and cutoff velocity is drawn as a dotted vertical line. Cutoff velocity is defined as

$$v_c = v_0 + \frac{1}{2}\frac{u_1^2}{\lambda_{mfp}}\frac{r-1}{r}\frac{r_{mag}^2}{r+r_{mag}^2}t_{acc}. \tag{24}$$

The derivation of the cutoff velocity is done in detail in Appendix B.

4 Results

4.1 Code validation

The simulation code has to be tested to verify its correct behaviour before any new simulation results can be discussed. To test the code a series of simulations with no ripples is done to check against the analytical solution of the power law equation (9). The Equation (9) depends only on the gas compression ratio.

The Figure 7 shows four plots with changing gas compression ratio and mean obliquity angle. On all of the panels the half dotted vertical line is the particle starting velocity and the dotted vertical line is the cutoff velocity 24. The top left panel shows a parallel shock with gas compression ratio of 3.0 and the top right panel shows a parallel shock with gas compression ratio of 4.0. The bottom left panel shows a mean obliquity 20.0 degrees shock with gas compression ratio of 3.0 and the bottom right panel shows a mean obliquity 20.0 degrees shock with gas compression ratio of 4.0. The spectra is compared to the power law equation (23) in each panel which is shown as a black dotted line.

As can be seen in the Figure 7 the simulation results mostly agree with the power law equation. There is a slight disagreement close to the particle starting velocity and close to the cutoff velocity. The difference close to the particle starting velocity is an artefact produced by the simulation since it uses a finite timestep.[Birdsall and Langdon, 2018]

From Figure 7 we can conclude that the simulation is working as intended. Increasing the shock normal angle accelerates particles to higher maximum energy and the results agree with the analytical solution to a reasonable degree.

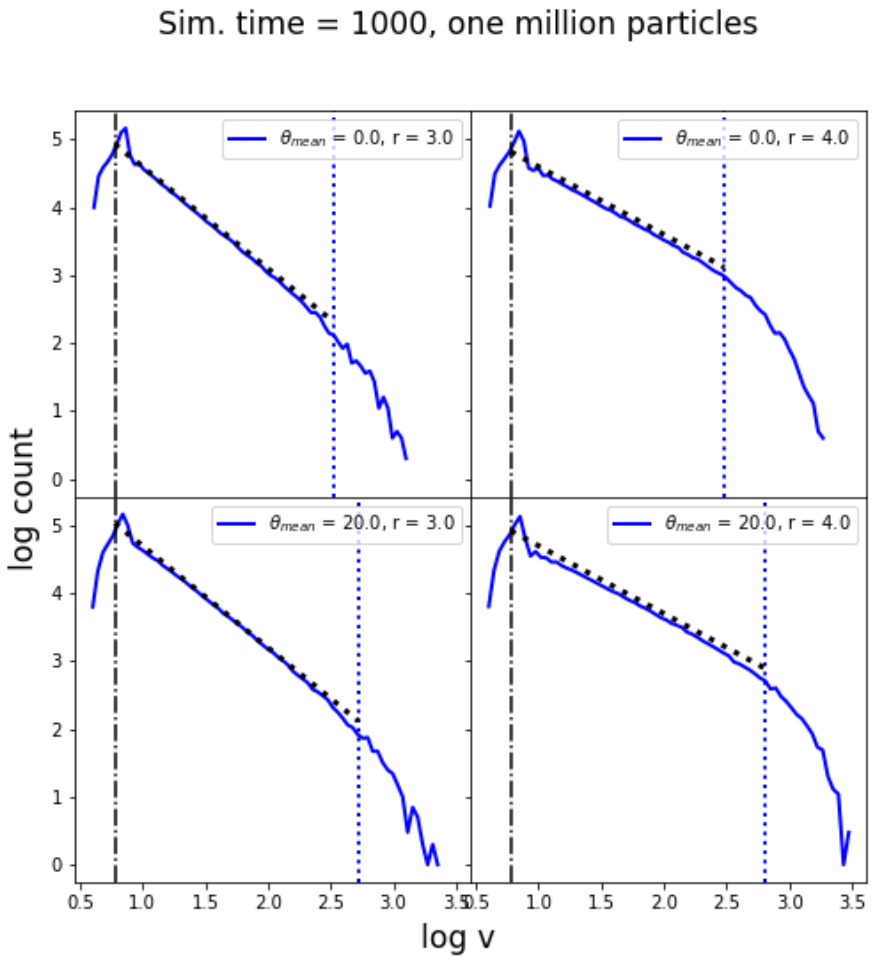

Figure 7. Four different shock simulations in blue compared to the black dotted power law of the analytical solution in Equation (9). The black vertical line is the initial velocity of the particles and the blue dotted line is the cutoff velocity of the simulation. Top row has parallel shocks and the bottom row has 20.0 degree obliquity shock. Left column has gas compression ratio of 3.0 and right column has gas compression ratio of 4.0.

4.2 The effects of ripples on a shock surface to particle acceleration

As discussed in section 3.2, the ripple in the simulations is controlled with five different parameters: ripple probability (how often the ripple is present when a particle is crossing the shock), ripple amplitude and wavelength (how big the ripple is) and ripple velocity in the x-plane and y-plane. The ripple velocity parameter is not explored in this thesis due to time restrictions.

In Figure 8 are the results of five simulations where the only changing parameter was the ripple amplitude. A parallel shock with a ripple probability of 40% and gas compression ratio of 8.0 was simulated each time with a different ripple amplitude. In the Figure are simulations for ripple amplitudes of 0.0, 0.1, 0.2, 0.3 and 0.4 which correspond to maximum shock angles of 0, 32.1, 51.5, 62.1 and 68.3 degrees. The notable change in the spectra is that the larger ripple amplitude simulations have less particles in the power law range and more particles are slower than the particle starting speed. The particle spectrum of the five simulations seem to suggest that the bigger the ripple amplitude the more slowing down of particles is happening and nothing changes in the power law spectrum ranges or at the higher energies, or tail, of the spectra.

The Figure 9 shows five different simulations where gas compression ratio is 8.0 and all other parameters were unchanged except for the ripple probability. The simulations had a parallel shock with a large ripple amplitude of 0.15 corresponding to a maximum angle of 43.3 degrees. The different ripple probabilities of the simulations were 0%, 30%, 50%, 70% and 100%. From the results we can see that increasing the ripple probability doesn't seem to effect the particle spectrum at the lower energies at all and only extends the tail of the spectrum as the probability increases.

To understand how the ripple probability changes the particle energy spectrum, a 100% probability rippled shock is compared to different non rippled shocks with

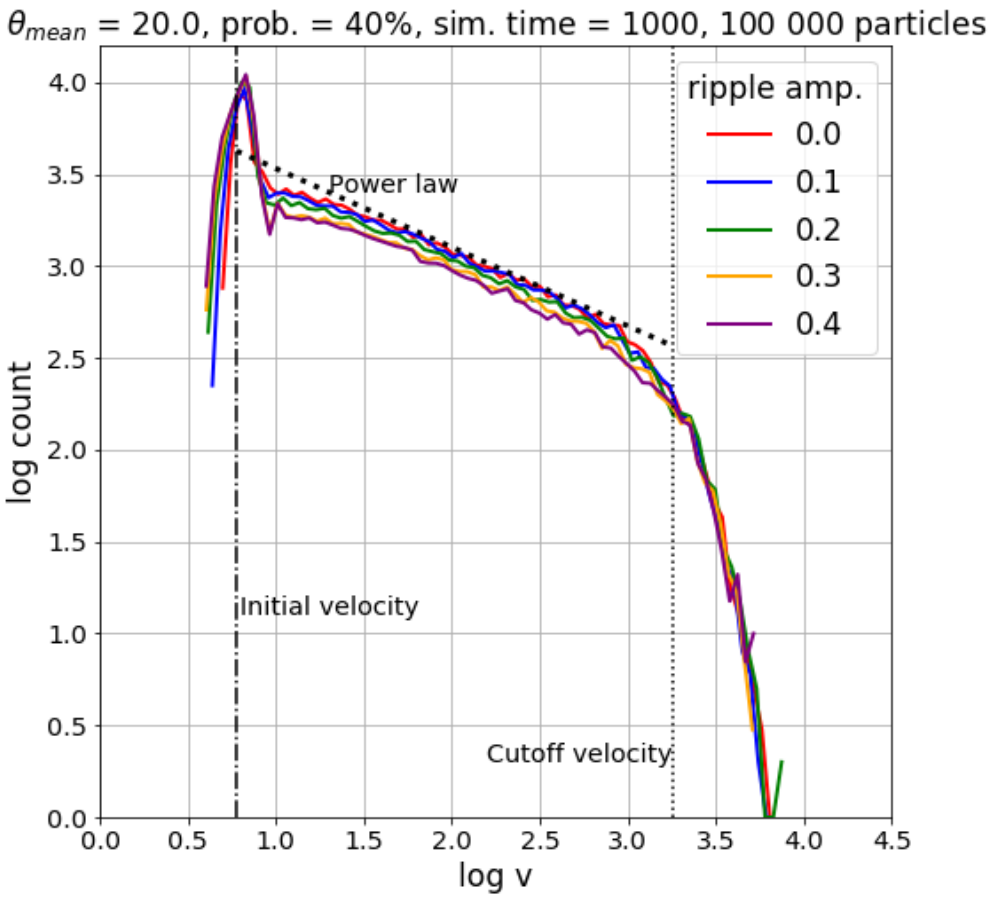

Figure 8. In this plot are results of simulations with gas compression ratio 8.0 and all parameters the same except for the ripple amplitude.

different mean obliquity angles. Figure 10 shows a rippled shock with mean obliquity angle of 20 degrees and and a ripple with amplitude 0.4 to have as large of an ripple as possible. The other three plots are non rippled shocks with mean obliquity angles of the same as the rippled shock (20.0°), the same as the minimum angle achieved with the ripple (0.08°) and the maximum angle achieved with the ripple (88.3°). The colour coded dotted vertical lines are the cutoff velocities of each non rippled shock. From the Figure we see that the rippled shock follows almost identically the 88.3 degree non rippled shock while 20.0 degree and 0.08 degree shocks have noticeably

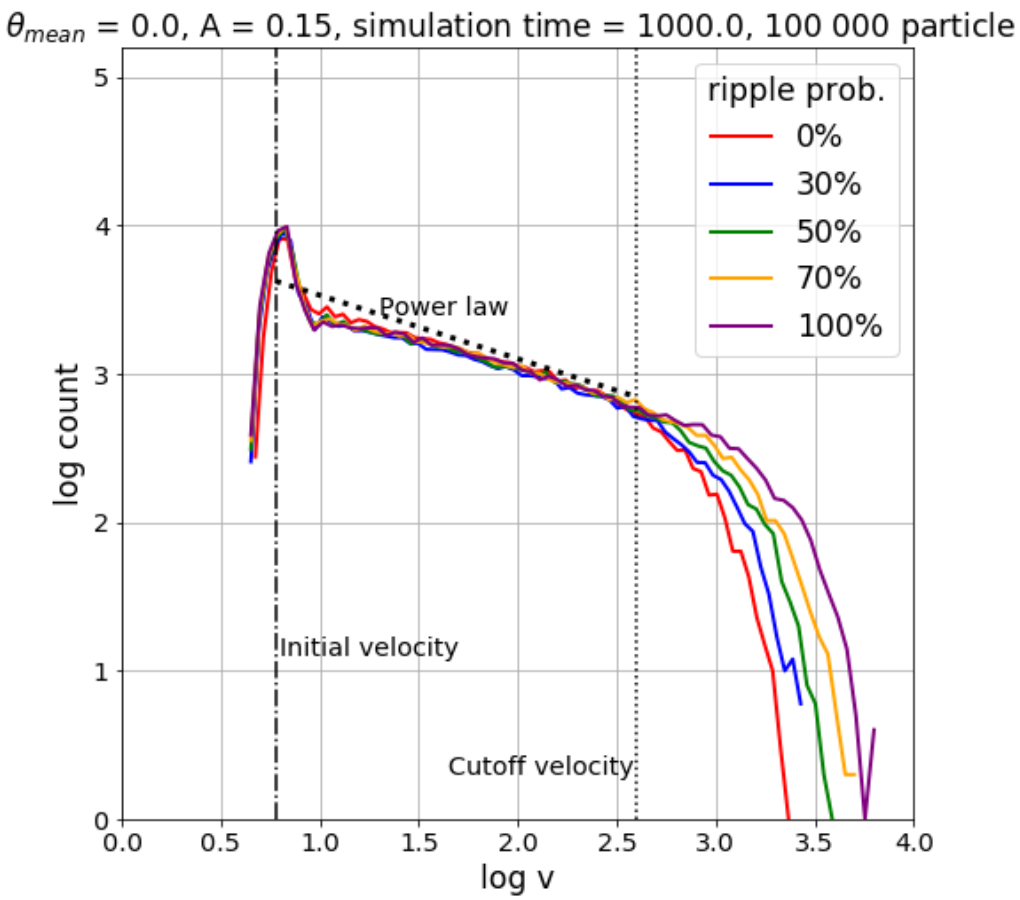

Figure 9. In this plot are results of simulations with gas compression ratio 8.0 and all parameters the same except for the ripple probability.

different tails. Also the power law spectrum is softer with the rippled shock and 88.3 degree non rippled shock than with the 0.08 and 20.0 degree shocks.

The same simulations from Figure 10 are used in Figure 11 but instead of the particle energy spectra the ending positions of particles is shown. In the Figure 11 we can see that in the most parallel shock most of the particles stay close to the shock and increasing the mean obliquity angle increases the amount of particles further away from the shock. With all the non rippled shocks the particles are evenly distributed to all distances from the shock until some steep drop off after

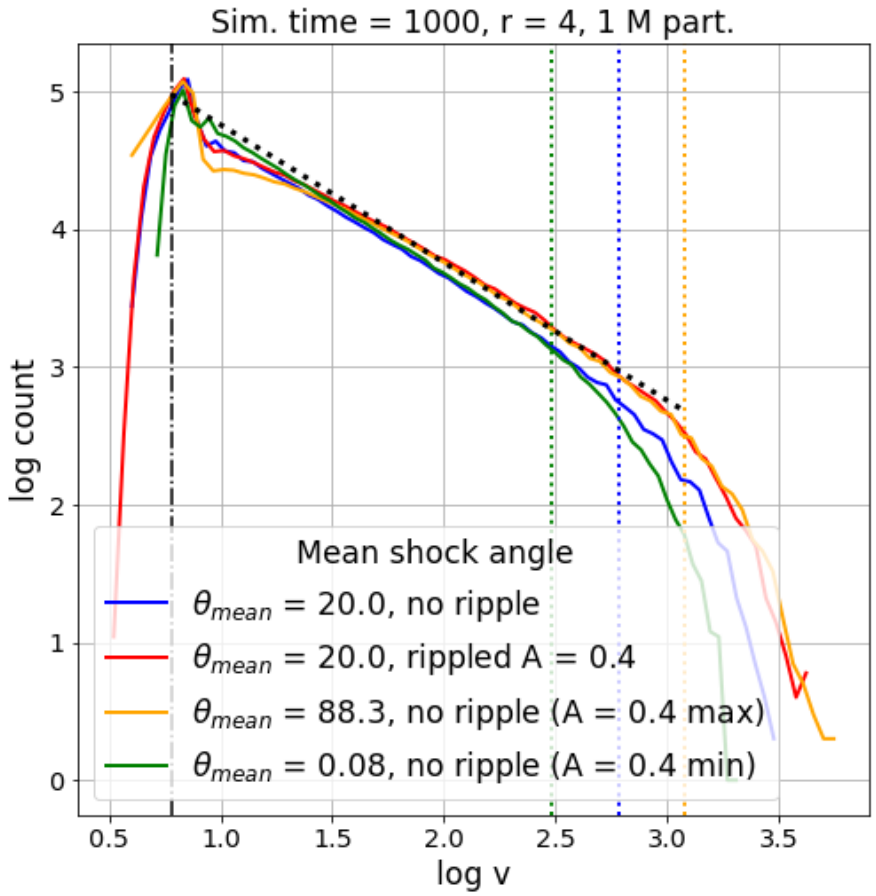

Figure 10. In this plot are results of simulations a rippled shock with non rippled shocks at different obliquities compared to the ripple.

which only a handful of particles in each simulation has reached. In the 20.0 degree rippled simulation there are almost the same amount of particles close to the shock as in the non rippled 20.0 degree case but instead of a steep drop off of particles at a certain distance there is a smoother decent into the larger distances from the shock.

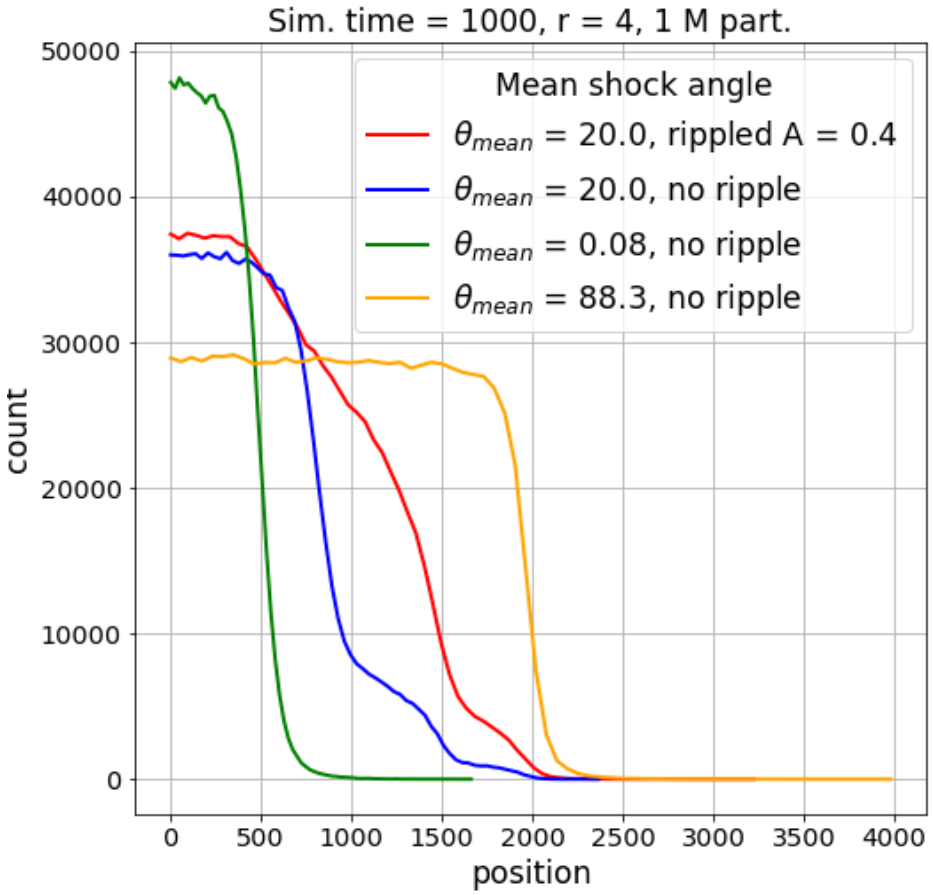

Figure 11. Downstream distribution of particles in the simulations shown in Figure 10.

5 Discussion

The main result in this thesis is seen in Figure 10. The Figure 10 shows that quasi-parallel shocks with ripples can accelerate particles as efficiently as perpendicular shocks. The other results are complementary to this main point. Figure 11 shows that the rippled shock does not accelerate the particles identically to the perpendicular shock, but the distribution of ending positions of the particles is more similar to the quasi-parallel shock with some outlier particles. From Figures 8 and 9 we can see that changing the amplitude does not change the particle spectra significantly, but the probability of the ripple being present is very important.

Giacalone and Neugebauer [2008] showed that a ripple with the same scale as the distance between two observers is able to affect the acceleration process of particles so that the single point observations were contradictory to theoretical prediction based on the local plasma properties. They concluded that the particle spectra is determined by the average gas compression ratio. The results of this thesis indicate that the resulting particle spectra relies heavily on the maximum shock normal angle achievable with the ripples and the proportion of time the ripples are present on the shock surface. In-situ observations of these parameters require a lot of measurements, either statistically or with a constellation mission with multiple small satellites. MMS mission observations have studied parallel shock ripples in the ion kinetic scale and found that temporal evolution of the ripple plays also a key role in the particle acceleration process [Gingell et al., 2017]. The simulation in this thesis is not able to evolve the ripple over time and thus study the small scale ripples in detail.

The simulation uses the guiding center approximation, which limits the minimum size of the ripples in the simulation to the ion gyroradius. But this is not such a big problem since ripples appear at various length scales and satellite observations have only recently been able to study ripples in the ion gyroradius scale [Johlander

et al., 2016]. Also using the guiding center approximation gives the code a fast iteration time from simulation to result. A bigger problem with the code is that the results are saved as a list and only in the end written to binary format. In the next version of the code this should be redone so that the code writes the results of the simulation in manageable chunks to file and flushes the random-access memory (RAM) after each write. Currently it really starts to fill up the RAM of even larger computational setups, with as low as ten million particles. This limits the number of particles the code can simulate and means that it is very limited in its ability to study the highest energy particles.

6 Conclusion and outlook

This thesis developed a simulation code to study the effect ripples have on particle acceleration. The simulation was a Monte Carlo test particle simulation, where the ripple was added on the shock surface. Having full control over the ripple provided the ability to isolate single parameters of the ripple and study the effects of parameters separately. And even though it is still too early to give definite answers to the importance of ripples, the results of this thesis show that there is clearly some effect the ripples are having on the acceleration of particles in shocks.

The results show that a quasi-parallel shock with a constantly present ripple was able to accelerate particles as efficiently as a quasi-perpendicular shock. Confirmation of these simulation results require in-situ observations by multi-spacecraft missions like the MMS or Cluster mission.

There is still a lot of future work to do in the realm of rippled shock simulations. Already within this thesis and its simulation code there are multiple opportunities. In the future, the code developed in this thesis could be used to study the effect of ripple velocities. This possibility is already implemented. The code could also be used to study different parameter combinations. There are different, more accurate and computationally expensive, ways the crossing of the ripple could be implemented in the simulation. The simulation code is completely numerical and use of physical units would give much easier to grasp results. The results of simulations with rippled shocks with physical units could be compared to real world observations further increasing our understanding of the ripples effect on particle acceleration.

Acknowledgements

This work was supported by the Jenny and Antti Wihuri Foundation and the Turku Collegium for Science and Medicine. The code used in this thesis is publicly available at https://github.com/SjobFra/rippled-shock-simulation.

References

Allen, M. P. and Tildesley, D. J.: Computer Simulation of Liquids, vol. 1, Oxford University Press, https://doi.org/10.1093/oso/9780198803195.001.0001, 2017.

Axford, W. I., Leer, E., and Skadron, G.: The Acceleration of Cosmic Rays by Shock Waves, in: International Cosmic Ray Conference, vol. 11 of *International Cosmic Ray Conference*, p. 132, 1977.

Baker, D., Riesberg, L., Pankratz, C., Panneton, R., Giles, B., Wilder, F., and Ergun, R.: Magnetospheric multiscale instrument suite operations and data system, Space Science Reviews, 199, 545–575, 2016.

Bale, S. D., Reiner, M. J., Bougeret, J. L., Kaiser, M. L., Krucker, S., Larson, D. E., and Lin, R. P.: The source region of an interplanetary type II radio burst, Geophysical Research Letters, 26, 1573–1576, https://doi.org/10.1029/1999GL900293, 1999.

Bell, A. R.: The acceleration of cosmic rays in shock fronts – I, Monthly Notices of the Royal Astronomical Society, 182, 147–156, https://doi.org/10.1093/mnras/182.2.147, 1978a.

Bell, A. R.: The acceleration of cosmic rays in shock fronts - II, Monthly Notices of the Royal Astronomical Society, 182, 443–455, https://doi.org/10.1093/mnras/182.3.443, 1978b.

Birdsall, C. and Langdon, A.: Plasma Physics via Computer Simulation, vol. 42, CRC Press, https://doi.org/10.1201/9781315275048, 2018.

Blandford, R. D. and Ostriker, J. P.: Particle acceleration by astrophysical shocks., apjl, 221, L29–L32, https://doi.org/10.1086/182658, 1978.

Bothmer, V. and Daglis, I.: Space Weather: Physics and Effects, Springer Praxis Books, Springer Berlin Heidelberg, 2007.

Büchner, J.: Vlasov-code simulation, in: Proceedings of ISSS, vol. 7, pp. 26–31, 2005.

Burgess, D. and Scholer, M.: Collisionless Shocks in Space Plasmas, Cambridge University Press, Cambridge, https://doi.org/10.1017/CBO9781139044097, 2015.

De Hoffmann, F. and Teller, E.: Magneto-Hydrodynamic Shocks, Phys. Rev., 80, 692–703, https://doi.org/10.1103/PhysRev.80.692, 1950.

Ellison, D. C.: Monte Carlo simulation of charged particles upstream of the Earth's bow shock, Geophysical Research Letters, 8, 991–994, 1981.

Forman, M. and Morfill, G.: Time-dependent acceleration of solar wind plasma to MeV energies at corotating interplanetary shocks, in: International Cosmic Ray Conference, vol. 5, p. 328, 1979.

Gary, S. P. and Gary, S. P.: Theory of space plasma microinstabilities, 7, Cambridge university press, 1993.

Giacalone, J. and Neugebauer, M.: The Energy Spectrum of Energetic Particles Downstream of Turbulent Collisionless Shocks, The Astrophysical Journal, 673, 629–636, https://doi.org/10.1086/524008, 2008.

Gingell, I., Schwartz, S. J., Burgess, D., Johlander, A., Russell, C. T., Burch, J. L., Ergun, R. E., Fuselier, S., Gershman, D. J., Giles, B. L., Goodrich, K. A., Khotyaintsev, Y. V., Lavraud, B., Lindqvist, P. A., Strangeway, R. J., Trattner, K., Torbert, R. B., Wei, H., and Wilder, F.: MMS Observations and Hybrid Simulations of Surface Ripples at a Marginally Quasi-Parallel Shock, Journal of Geophysical Research: Space Physics, 122, 11,003–11,017, https://doi.org/10.1002/2017JA024538, 2017.

Gombosi, T.: Physics of the Space Environment, Cambridge Atmospheric and Space Science Series, Cambridge University Press, 1998.

Hietala, H. and Plaschke, F.: On the generation of magnetosheath high-speed jets by bow shock ripples, Journal of Geophysical Research: Space Physics, 118, 7237–7245, https://doi.org/10.1002/2013JA019172, 2013.

Huang, K.: Introduction to Statistical Physics, Second Edition, Civil and Environmental Engineering, CRC Press, 2009.

Johlander, A., Schwartz, S. J., Vaivads, A., Khotyaintsev, Y. V., Gingell, I., Peng, I. B., Markidis, S., Lindqvist, P. A., Ergun, R. E., Marklund, G. T., Plaschke, F., Magnes, W., Strangeway, R. J., Russell, C. T., Wei, H., Torbert, R. B., Paterson, W. R., Gershman, D. J., Dorelli, J. C., Avanov, L. A., Lavraud, B., Saito, Y., Giles, B. L., Pollock, C. J., and Burch, J. L.: Rippled quasiperpendicular shock observed by the magnetospheric multiscale spacecraft, Physical Review Letters, 117, 1–5, https://doi.org/10.1103/PhysRevLett.117.165101, 2016.

Kallenrode, M.-B.: Space Physics, vol. 88 of *Advanced Texts in Physics*, Springer Berlin Heidelberg, Berlin, Heidelberg, https://doi.org/10.1007/978-3-662-09959-9, 2004.

Krishan, V.: Two-Fluid Description of Plasmas, pp. 197–234, Springer Netherlands, Dordrecht, https://doi.org/10.1007/978-94-011-4720-0_5, 1999.

Krymskii, G. F.: A regular mechanism for the acceleration of charged particles on the front of a shock wave, Akademiia Nauk SSSR Doklady, 234, 1306–1308, 1977.

Landau, L. and Lifshitz, E.: Fluid Mechanics: Volume 6, vol. 6, Elsevier Science, 1987.

Lowe, R. E. and Burgess, D.: The properties and causes of rippling in quasi-perpendicular collisionless shock fronts, Annales Geophysicae, 21, 671–679, https://doi.org/10.5194/angeo-21-671-2003, 2003.

Lucek, E. A., Horbury, T. S., Dandouras, I., and Rème, H.: Cluster observations of the Earth's quasi-parallel bow shock, Journal of Geophysical Research: Space Physics, 113, https://doi.org/10.1029/2007JA012756, 2008.

Morse, R. L. and Nielson, C. W.: Numerical Simulation of Warm Two-Beam Plasma, The Physics of Fluids, 12, 2418–2425, https://doi.org/10.1063/1.1692361, 1969.

Neugebauer, M. and Giacaione, J.: Multi-spacecraft observations of interplanetary shocks: Non-planarity and energetic particles, European Space Agency, (Special Publication) ESA SP, 110, 101–105, https://doi.org/10.1029/2005JA011380, 2005.

Páez, A., Jatenco-Pereira, V., Falceta-Gonçalves, D., and Opher, M.: Corrugated Features in Coronal-mass-ejection-driven Shocks: A Discussion on the Predisposition to Particle Acceleration, The Astrophysical Journal, 879, 122, https://doi.org/10.3847/1538-4357/ab2460, URL http://dx.doi.org/10.3847/1538-4357/ab2460, 2019.

Palmroth, M., Ganse, U., Pfau-Kempf, Y., Battarbee, M., Turc, L., Brito, T., Grandin, M., Hoilijoki, S., Sandroos, A., and von Alfthan, S.: Vlasov methods in space physics and astrophysics, Living Reviews in Computational Astrophysics, 4, https://doi.org/10.1007/s41115-018-0003-2, 2018.

Piel, A.: Plasma physics: an introduction to laboratory, space, and fusion plasmas, Springer, 2017.

Scudder, J. D., Mangeney, A., Lacombe, C., Harvey, C. C., and Aggson, T. L.: The resolved layer of a collisionless, high β, supercritical, quasi-perpendicular shock wave, 2. Dissipative fluid electrodynamics, Journal of Geophysical Research: Space Physics, 91, 11 053–11 073, https://doi.org/10.1029/JA091iA10p11053, 1986a.

Scudder, J. D., Mangeney, A., Lacombe, C., Harvey, C. C., Aggson, T. L., Anderson, R. R., Gosling, J. T., Paschmann, G., and Russell, C. T.: The resolved layer of a collisionless, high β, supercritical, quasi-perpendicular shock wave: 1. Rankine-Hugoniot geometry, currents, and stationarity, Journal of Geophysical Research: Space Physics, 91, 11 019–11 052, https://doi.org/10.1029/JA091iA10p11019, 1986b.

Scudder, J. D., Mangeney, A., Lacombe, C., Harvey, C. C., Wu, C. S., and Anderson, R. R.: The resolved layer of a collisionless, high β, supercritical, quasi-perpendicular shock wave: 3. Vlasov electrodynamics, Journal of Geophysical Research: Space Physics, 91, 11 075–11 097, https://doi.org/10.1029/JA091iA10p11075, 1986c.

Sugiyama, T. and Terasawa, T.: A scatter-free ion acceleration process in the parallel shock, Advances in Space Research, 24, 73 – 76, https://doi.org/https://doi.org/10.1016/S0273-1177(99)00427-5, 1999.

Susino, R., Bemporad, A., and Mancuso, S.: Physical Conditions of Coronal Plasma at the Transit of a Shock Driven by a Coronal Mass Ejection, apj, 812, 119, https://doi.org/10.1088/0004-637X/812/2/119, 2015.

Vainio, R.: Diffusive Shock Acceleration, in: Plasma Turbulence and Energetic Particles in Astrophysics, edited by Ostrowski, M. and Schlickeiser, R., pp. 232–245, 1999.

Wertz, J. and Larson, W.: Space Mission Analysis and Design, Space Technology Library, Springer Netherlands, 1999.

Winske, D. and Omidi, N.: A nonspecialist's guide to kinetic simulations of space plasmas, Journal of Geophysical Research: Space Physics, 101, 17 287–17 303, https://doi.org/10.1029/96JA00982, 1996.

Winske, D. and Quest, K. B.: Magnetic field and density fluctuations at perpendicular supercritical collisionless shocks, Journal of Geophysical Research: Space Physics, 93, 9681–9693, https://doi.org/10.1029/JA093iA09p09681, 1988.

Appendices

This thesis is a part of a larger, Jenny and Antti Wihuri Foundation funded project in the University of Turku called "Hiukkaskiihdytys avaruuden shokkiaalloissa: shokkipinnan väreilyn vaikutus". The derivation of Appendix A was done as a part of this study by Prof. Rami Vainio and Dr. Alexandr Afanasiev and is used in this thesis to simulate the ripples. The derivation uses two random numbers to calculate a random point on a sinusoidal surface.

The derivation of Appendix B was done by Prof. Rami Vainio using Vainio [1999] as a starting point for instantaneous release case. The derivation was adapted for continuous release for the simulation in this thesis by Dr. Alexandr Afanasiev.

A Picking a random point on a rippled surface

A sinusoidal rippled surface with mean normal in the z direction can be given as

$$0 = f(x, y, z) = z - A \sin kx \sin ky,$$

where $k = 2\pi/\lambda_{wl}$ is the characteristic wavenumber of the ripple and λ_{wl} is its characteristic length scale, has a normal

$$\begin{aligned} \boldsymbol{n} &= \frac{\nabla f}{|\nabla f|} \\ \nabla f &= -Ak(\cos kx \sin ky \boldsymbol{e}_x + \sin kx \cos ky \boldsymbol{e}_y) + \boldsymbol{e}_z \\ |\nabla f| &= \sqrt{A^2k^2(\cos kx^2 \sin ky^2 + \sin kx^2 \cos ky^2 + 1.} \end{aligned}$$

Thus, the components of the normal vector can be obtained from

$$\begin{aligned} n_x &= -\frac{Ak \cos kx \sin ky}{\sqrt{A^2k^2(\cos kx^2 \sin ky^2 + \sin kx^2 \cos ky^2) + 1}} \\ n_y &= -\frac{Ak \sin kx \cos ky}{\sqrt{A^2k^2(\cos kx^2 \sin ky^2 + \sin kx^2 \cos ky^2) + 1}} \\ n_z &= \frac{1}{\sqrt{A^2k^2(\cos kx^2 \sin ky^2 + \sin kx^2 \cos ky^2) + 1}}. \end{aligned}$$

We can normalize the units of length to λ_{wl}, whence

$$n_x = -\frac{a\cos 2\pi x \sin 2\pi y}{\sqrt{a^2(\cos 2\pi x^2 \sin 2\pi y^2 + \sin 2\pi x^2 \cos 2\pi y^2) + 1}}$$
$$n_y = -\frac{a\sin 2\pi x \cos 2\pi y}{\sqrt{a^2(\cos 2\pi x^2 \sin 2\pi y^2 + \sin 2\pi x^2 \cos 2\pi y^2) + 1}}$$
$$n_z = \frac{1}{\sqrt{a^2(\cos 2\pi x^2 \sin 2\pi y^2 + \sin 2\pi x^2 \cos 2\pi y^2) + 1}}.$$

Thus, choosing $x, y \in [0, 1)$ randomly from uniform distribution allows one to derive the components of the randomly fluctuating $\boldsymbol{n}$, given the value of $a = 2\pi A/\lambda_{wl}$. Assuming further that the upstream magnetic field is in the xz plane allows one to define the unit vector of the $\boldsymbol{B}$ field as

$$\boldsymbol{b} = \cos\Theta_{B<\boldsymbol{n}>}\boldsymbol{e}_z + \sin\Theta_{B<\boldsymbol{n}>}\boldsymbol{e}_x.$$

This then gives

$$\cos\Theta_{Bn} = \boldsymbol{n}\cdot\boldsymbol{b} = \frac{\cos\Theta_{B<\boldsymbol{n}>} - a\sin\Theta_{B<\boldsymbol{n}>}\cos 2\pi x \sin 2\pi y}{\sqrt{a^2(\cos 2\pi x^2 \sin 2\pi y^2 + \sin 2\pi x^2 \cos 2\pi y^2) + 1}}. \tag{25}$$

This equation would be strictly valid at the limit of $a \to 0$, i.e., if the intersection of the magnetic field line and the shock surface is almost at $z = 0$. However, we can also solve the actual intersection point numerically. The equation governing it can be obtained by choosing the magnetic field line to intersect the xy plane in a random point (x_0, y_0). Thus, the equations of the field line are

$$z = \cot\Theta_{B<\boldsymbol{n}>}(x - x_0).$$
$$y = y_0$$

Combining these with the equation of the rippled surface gives (in our dimensionless unit system where $\lambda_{wl} = 1$, i.e., $A = a/2\pi$)

$$\frac{a}{2\pi}\sin 2\pi x \sin 2\pi y_0 = \cot\Theta_{B<\boldsymbol{n}>}(x - x_0)$$

giving

$$x = x_0 + \frac{a}{2\pi}\tan\Theta_{B<\boldsymbol{n}>}\sin 2\pi y_0 \sin 2\pi x, \tag{26}$$

which for small values of $(a/2\pi)\tan\Theta_{B<\boldsymbol{n}>}\sin 2\pi y_0$ can be solved iteratively as

$$x^{(n+1)} = x_0 + \frac{a}{2\pi}\tan\Theta_{B<\boldsymbol{n}>}\sin 2\pi y_0 \sin 2\pi x^{(n)}$$
$$x^{(0)} = x_0,$$

but in any case numerically. Thus, one should first choose $x_0, y_0 \in [0, 1)$ randomly, then use $y = y_0$ and compute the value of x as a function of x_0 and y_0 from Equation (26) and then substitute them to Equation (25).

Then next task is to compute the speed of the field line intersection point along the magnetic field, if the rippled surface is moving in the lateral direction in the undisturbed de Hoffmann-Teller frame. Now, the surface is moving so its equation is

$$z = \frac{a}{2\pi} \sin 2\pi(x - V_x t) \sin 2\pi(y - V_y t),$$

where the ripple velocity is

$$\boldsymbol{V} = V_x \boldsymbol{e}_x + V_y \boldsymbol{e}_y.$$

The point of intersection, thus, is moving at velocity

$$\delta \boldsymbol{u}_1 = \dot{x} \boldsymbol{e}_x + \dot{z} \boldsymbol{e}_z,$$

where

$$\dot{x} = \dot{z} \tan \Theta_{B<\boldsymbol{n}>}$$
$$\dot{z} = a[(\dot{x} - V_x) \cos 2\pi(x - V_x t) \sin 2\pi(y_0 - V_y t) - V_y(\sin 2\pi(x - V_x t) \cos 2\pi(y_0 - V_y t)].$$

Without the loss of generality (as we draw x_0 and y_0 randomly), we can evaluate the velocity components at time $t = 0$ and the solution is

$$\dot{x} = \frac{a \tan \Theta_{B<\boldsymbol{n}>}}{a \tan \Theta_{B<\boldsymbol{n}>} \cos 2\pi x \sin 2\pi y_0 - 1} [V_x \cos 2\pi x \sin 2\pi y_0 + V_y \sin 2\pi x \cos 2\pi y_0]$$
$$\dot{z} = \frac{\dot{x}}{\tan \Theta_{B<\boldsymbol{n}>}}$$

and x needs to be solved from Equation (26). A positive value for $\dot{z}$ (and, thus, $\dot{x}$) implies that the intersection point is moving upwards, which implies an increase in the local de Hoffmann-Teller frame fluid velocity. Thus, the change in the local de Hoffmann-Teller fluid velocity is

$$\delta u_1 = \frac{a(V_x \cos 2\pi x \sin 2\pi y_0 + V_y \sin 2\pi x \cos 2\pi y_0)}{a \sin \Theta_{B<\boldsymbol{n}>} \cos 2\pi x \sin 2\pi y_0 - \cos \Theta_{B<\boldsymbol{n}>}}. \tag{27}$$

We have calculated this in dimensionless units, but as the result is directly proportional to the velocity of the ripple, the same applies in the physical units as well.

B Acceleration of particles in a finite time simulation

Acceleration time in diffusive shock acceleration from momentum p_0 to p is

$$\tau(p) = \frac{3}{u_{x,1} - u_{x,2}} \int_{p_0}^{p} \frac{\mathrm{d}p}{p} \left(\frac{D_{xx,1}}{u_{x,1}} + \frac{D_{xx,2}}{u_{x,2}} \right), \tag{28}$$

where $D_{xx} = \frac{1}{3}\lambda_{mfp}\Theta_{B_n}$ is the diffusion coefficient in the shock-normal direction x, λ_{mfp} is the parallel mean free path, and $u_x = u\cos\Theta_{B_n}$ the bulk velocity component in the shock normal direction. Here we have assumed that particles propagate along the magnetic field and ignore perpendicular diffusion entirely.

Thus, the acceleration rate for a constant parallel mean free path, $\lambda_{mfp,1} = \lambda_{mfp,2} = \lambda_{mfp,3}$ is

$$\begin{aligned}
\frac{1}{p}\frac{\mathrm{d}p}{\mathrm{d}t} &= \frac{u_{x,1} - u_{x,2}}{3} \left(\frac{D_{xx,1}}{u_{x,1}} + \frac{D_{xx,2}}{u_{x,2}} \right)^{-1} \\
&= \frac{u_{x,1}(r-1)}{r} \frac{3}{\lambda_{mfp} v} \left(\frac{\cos\Theta_{B_n,1}}{u_1} + \frac{\cos\Theta_{B_n,2}}{u_2} \right)^{-1} \\
&= \frac{u_1^2(r-1)}{r} \frac{1}{\lambda_{mfp} v} \left(1 + \frac{u_1}{u_2}\frac{\cos\Theta_{B_n,2}}{\cos\Theta_{B_n,1}} \right)^{-1} \\
&= \frac{1}{v}\frac{u_1^2}{\lambda_{mfp}}\frac{r-1}{r} \left(1 + \frac{r}{r_B}\frac{B_x/B_2}{B_x/B_1} \right)^{-1} \\
&= \frac{1}{v}\frac{u_1^2}{\lambda_{mfp}}\frac{r-1}{r} \left(1 + \frac{r}{r_B^2} \right)^{-1} \\
&= \frac{1}{v}\frac{u_1^2}{\lambda_{mfp}}\frac{r-1}{r}\frac{r_B^2}{r + r_B^2}.
\end{aligned}$$

Therefore, at non-relativistic speeds, where $\dot{p}/p = \dot{v}/v$, particles gain speed at rate

$$\frac{\mathrm{d}v}{\mathrm{d}t} = \frac{u_1^2}{\lambda_{mfp}}\frac{r-1}{r}\frac{r_B^2}{r + r_B^2}$$

giving the characteristic speed the particles can get in t_{acc}, the time available for the acceleration process, as

$$v_c = v_0 + \frac{u_1^2}{\lambda_{mfp}}\frac{r-1}{r}\frac{r_B^2}{r + r_B^2} t_{acc}.$$

The continuous injection of particles during the whole simulation time t_{acc} can be taken into account in the following way:

$$v_c = v_0 + \int_0^1 \mathrm{d}\left(\frac{t'}{t_{\mathrm{acc}}}\right) \int_{t'}^{t_{\mathrm{acc}}} \mathrm{d}t \frac{u_1^2}{\lambda_{mfp}}\frac{r-1}{r}\frac{r_B^2}{r + r_B^2} = v_0 + \frac{1}{2}\frac{u_1^2}{\lambda_{mfp}}\frac{r-1}{r}\frac{r_B^2}{r + r_B^2} t_{\mathrm{acc}}.$$